

An *in-silico* Evaluation of Some Schiff bases for Their Potency Against SARS-CoV-2 Main Protease, PASS Prediction and ADMET Studies

Mohammad Nasir Uddin*, Md. Saiful Rahman

Department of Chemistry, University of Chittagong, Chittagong-4331, Bangladesh

Abstract

SARS-CoV-2 has created an agonizing pandemic situation all over the world. The inhibition of SARS-CoV-2 main protease (Mpro) by the blockage of viral replication is considered an important drug target to the many researchers working to discover specific drugs for COVID-19 treatment. Schiff bases being documented to possess antimicrobial properties might be investigated as the candidate against COVID-19. Bioactivities of some symmetrical bis-Schiff bases were evaluated using computational studies on the basis of binding affinity, PASS prediction and ADMET study. On the basis of binding affinity, it is concluded that among eighteen tested ligands 2, 5, 8, 16, 17 showed excellent, ligands 4, 6, 18 showed good and the remaining ligands showed moderate inhibition against SARS-CoV-2 Mpro (6LU7) compared to a prescribed anti-Covid-19 drug, hydroxychloroquine (HCO). PASS prediction revealed some of Schiff bases to have good anti-carcinogenic, anti-tuberculosis, antifungal, and antiviral activities. ADMET study predicted them to be non-toxic and harmless indicating that Schiff bases may act as a promising drug candidate for the treatment of COVID-19.

Keywords: Schiff-base, SARS-CoV-2 Mpro, Molecular Docking, PASS and ADMET Analysis

1. Introduction

At the end of 2019, a novel coronavirus disease (COVID-19) caused by severe acute respiratory syndrome coronavirus-2 (SARS-CoV-2) started in the city of Wuhan, China and then spread worldwide rapidly [1]. The virus, known as coronavirus, looks like crown-shaped spike glycoproteins and has a diameter of 60-140 nm under an electron microscope [2]. On the basis of the spreading rate, severity, infections and level of activity, the World Health Organization (WHO) declared the epidemic situation of COVID-19 a pandemic on 11th March 2020 [3]. Currently, more than 225 countries are affected by COVID-19 and the infections are still increasing exponentially. This coronavirus disease has not only challenged human health but also enormously affected the global economy [4]. COVID-19 caused by SARS CoV-2 contains two open reading frames (ORF1a and ORF1ab) [5]. These two ORFs play a key role in viral replication and transcription, translating two overlapping viral polyproteins (pp1a and pp1ab) [6]. During the proteolytic process, polyproteins released some functional polypeptides by the papain-like proteinase (PLpro) and the 3C-like protease (3CLpro). PLpro are responsible for the cleaving of three sites and 3CLpro for 11 sites respectively [7]. 3CLpro is known as main protease

* Corresponding author.

E-mail address: mnuchm@cu.ac.bd, nasircu72@gmail.com

Manuscript History:

Received 14 November, 2022, Revised 13 February, 2023, Accepted 27 March, 2023, Published 30 April, 2023

Copyright © 2023 UNIMAS Publisher. This is an open access article under the CC BY-NC-SA 4.0 license.

<https://doi.org/10.33736/jaspe.5133.2023>

(Mpro) due to most of the polypeptide site cleaves. It is reported that Mpro is a cysteine protease with a Cys-His catalytic dyad (His41 and Cys145) in the active site of the protease [8]. Mpro is considered an important target for antiviral drug design for the treatment of COVID-19 as it plays a key role in viral replication and maturation [9]. The hydroxychloroquine, an approved drug from Food and Drug Administration (FDA) for malaria disease, was explored for SARS-CoV-2 medication [10]. Based on previous reports, chloroquine and hydroxychloroquine can be used for coronavirus treatment having the p^H changing capacity at the surface of the cell membrane which can inhibit the virus to attach to the cell membrane. Prevention capacity of nucleic acid replication, virus assembly, virus release, glycosylation of viral proteins and new virus particle delivery supports antiviral effects [11]. Remdesivir is also an approved drug for Ebola's medication [12] that demonstrated activity against the coronavirus family in 2017 and 2020 [13]. Some protease inhibitors like ritonavir/lopinavir may also have an antiviral effect [14].

Schiff bases have wide applications in the food industry, dye industry, catalysis, fungicidal, agrochemical and biological activities [15]. Mesoporous silica-based nanocomposite materials were functionalized with some Schiff base ligands and were used for the determination and removal of trace amount of Cu(II), Pb(II), Pb(II), Hg(II), Pd(II) in the environmental samples [16-21]. Several Schiff bases are reported to possess remarkable antibacterial, antifungal, and anticancer activities due to their C=N moiety [15].

However, the vaccines have been determined to be safe for adults and they are being studied in children [22]. Again any virus changes or mutations may make vaccines ineffective [23]. While vaccinations reduce the incidence of SARS-CoV-2 infections, there is still a need for drugs that can treat people who have contracted the virus. However, several domestic and foreign research institutions are still trying to discover an effective drug or vaccine for COVID-19 treatment considering the risk factors associated with viral infection. In recent years, medicinal chemists have attracted their attention towards new chemotherapeutics. Schiff bases and their metal complexes owing to their numerous applications in pharmacology as antiviral, antibacterial, antifungal, antimalarial, antituberculosis, anticancer, anti-HIV, anti-inflammatory, and antipyretic agents. Schiff base ligands of isatin have been reported to have antiviral activities against Moloney leukemia virus, vaccinia, rhino virus and SARS virus [24]. Schiff bases derived from 5-acyl-1,2,4-triazines with oximes, hydrazone, semicarbazones, and thiosemicarbazones showed considerable antiviral activities [25]. *In silico* prediction of some tetradentate symmetrical bis-Schiff bases of 1,6-hexanediamine proved them to be potential inhibitor against coronavirus (SARS-CoV-2) [26].

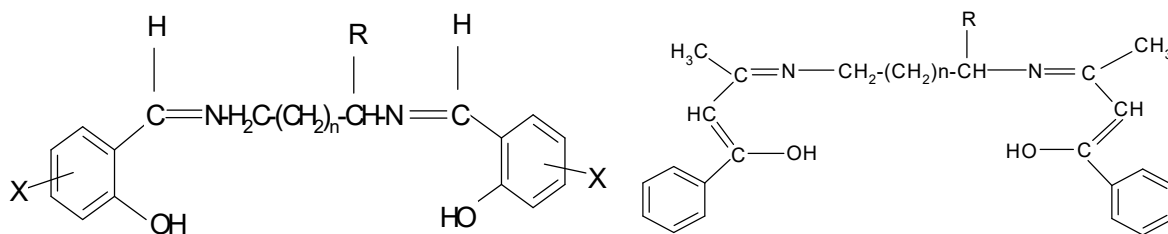
Thus, it is very much reasonable to search for newer anti-COVID-19 drug development. In this study, Density Functional Theory was employed to optimize some previously synthesized Schiff-base ligands [27-29] and to investigate their physicochemical properties. Molecular docking was performed to understand the binding affinity and interactions between ligands and receptor proteins. ADMET analysis was carried out to measure their biological position like absorption, metabolism and carcinogen.

2. Methods

2.1 Synthesis and characterization:

A total of 18 tetradentate symmetrical Schiff bases (ONNO) as shown in Figure 1 were obtained by the condensation of diamine (ethylenediamine, ED; 1,2 or 1,3-propanediamine, PD; 1,4-butanediamine, BD; 1,6-hexanediamine, HD and orthophenylenediamine, OPD) with methoxysalicylaldehyde (^MSal), 2-hydroxynaphthaldehyde (HNP) or benzoylacetone (BzA) in appropriate solvent either ethanol or methanol when the mixture was refluxed in the neutral medium [27-29]. The

structures of the ligands were previously established by their physical (melting point, color, yields, solubility), elemental (CHN) analysis, thermal analysis, magnetic susceptibility, electro-chemical (conductance measurements and cyclic voltammetry), and spectral (UV-visible, FTIR, ¹H NMR, and mass analysis) analytical techniques [27-29].



- | | | | | | |
|-----------|---------|--------------------------|----------------------|-----------|--|
| 1 | ED; | n=0, R=H, | X= CH ₃ O | | |
| 2 | ED; | n=0, R=H, | X= Fused Ph | 3 | BzA-ED-BzA, n=0, R=H |
| 4 | 1,2-PD; | n=0, R=CH ₃ , | X= CH ₃ O | 6 | BzA-1,2-PD-BzA, n=0, R=CH ₃ |
| 5 | 1,2-PD; | n=0, R=CH ₃ , | X= Fused Ph | 9 | BzA-1,3-PD-BzA, n=1, R=H |
| 7 | 1,3-PD; | n=1, R=H, | X= CH ₃ O | 12 | BzA-BD-BzA, n=2, R=H |
| 8 | 1,3-PD; | n=1, R=H, | X= Fused Ph | 15 | BzA-HD-BzA, n=4, R=H |
| 10 | 1,4-BD; | n=2, R=H, | X= CH ₃ O | | |
| 11 | 1,4-BD; | n=2, R=H, | X= Fused Ph | | |
| 13 | 1,6-HD; | n=4, R=H, | X= CH ₃ O | | |
| 14 | 1,6-HD; | n=4, R=H, | X= Fused Ph | | |

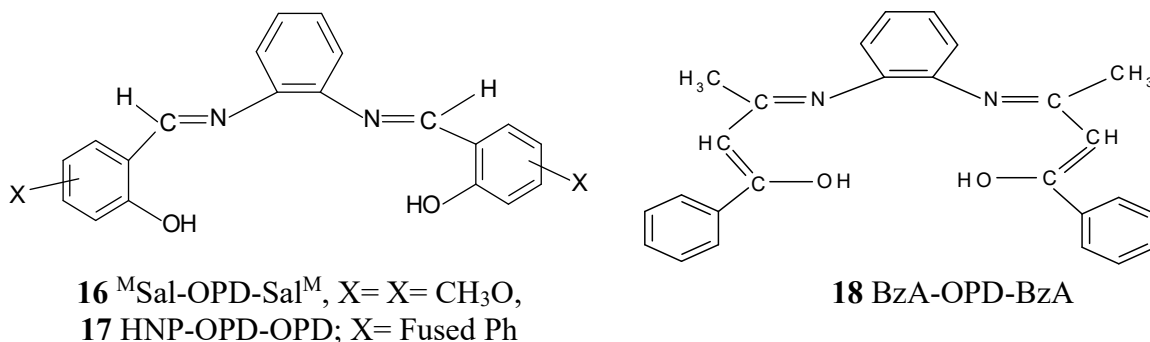


Figure 1. Structure of Schiff Bases (1-18) under investigation

2.2 Computational details

Optimization of Schiff-base ligands

In computer-aided drug design, the quantum chemical approach is widely used to investigate physicochemical properties like thermodynamic properties, molecular orbital features, dipole moment, and electrostatic potential [30]. A number of 22 ligands were selected considering their antiviral

activities. Each of the ligands was optimized with B3LYP hybrid functional parameter [31] under 6-31G (d, p) basis set for DFT calculations using Gaussian 09 program package [32]. All ligands were optimized in the gas phase. Physicochemical properties were also calculated at the same level as theory. HOMO-LUMO energy gap, hardness (η), softness (S) and chemical potential (μ) were calculated using HOMO and LUMO energies and considering Parr and Pearson interpretation [33] of DFT and Koopmans theorem [34] using the following equations:

$$\text{Gap } (\Delta E) = [\varepsilon_{\text{LUMO}} - \varepsilon_{\text{HOMO}}]; \eta = \frac{[\varepsilon_{\text{LUMO}} - \varepsilon_{\text{HOMO}}]}{2};$$

$$\mu = \frac{[\varepsilon_{\text{LUMO}} + \varepsilon_{\text{HOMO}}]}{2}; S = \frac{1}{\eta}$$

Preparation of protein for docking studies

The crystal structure (3D) of SARS Cov-2 Mpro (PDB ID: 6LU7) [35] was taken in pdb format from the protein data bank (PDB) and used as a receptor protein. Some significant factors like side chain geometry, missing hydrogen and improper bond order were observed in the crystal structure of 6LU7. PyMol (version 1.7) [36] software package was used to eliminate inhibitors, water molecules and hetero atoms present in 6LU7. The receptor protein was optimized and checked based on their least energy by Swiss-Pdb viewer (version 4.1.0) software [37]. Finally, the selected protein was ready to dock with optimized molecules considering molecule as ligand and protein as macromolecule.

Molecular docking analyses and visualization

In drug design, molecular docking simulation was carried out to obtain binding affinity and mode(s) of ligand and protein [38]. PyRx software (version 0.8) [39] was utilized to perform molecular docking of 6LU7 with optimized ligands individually. The center of the grid box was chosen targeting the active site of the main protease to be at x: -26.29, y: 12.60 and z: 58.96 respectively with a suitable grid box volume where the ligands be fitted easily. After that, structures of protein and ligand were saved in pdb format for non-bonding interactions. Non-bonding interactions were performed utilizing Accelrys Discovery Studio (version 4.5) [40] to analyze, visualize and differentiate interactions between ligands and amino acid residues of 6LU7.

PASS predication

PASS is a computer-based program used for the prediction of different types of pharmacological activities for different substances which was designed to anticipate a plethora of biological activities with 90% accuracy [41]. PASS prediction is based on structural activity relationship (SAR) analysis of the training set containing more than 205,000 compounds exhibiting more than 3750 kinds of biological activities. The predicted activity spectrum of a compound is estimated as probable activity (Pa) and probable inactivity (Pi). The scale of which is 0.000 to 1.000. Generally, it is considered that $Pa > Pi$ and $Pa + Pi \neq 1$. The compounds showing more Pa value than Pi are the only constituents considered as possible for a particular pharmacological activity [43].

ADMET prediction

Toxicity and some pharmacokinetic parameters of selected ligands were predicted utilizing AdmetSAR online database [43]. Nowadays, ADMET prediction assists scientists and researchers to identify safe and effective drug candidates. The result was observed by utilizing both SDF (Structure Data File) and SMILES (simplified molecular-input line-entry system) strings.

3. Results

3.1 Thermodynamic properties analysis

The theoretical DFT calculations were carried out employing 6-31G (d, p) basis set in the gas phase and the obtained result of thermal parameters like enthalpy, free energy and dipole moment are summarized in Table 1. The optimized structures of selected ligands (1-18) are depicted in Figure 2. The reaction spontaneity and product stability can be predicted through enthalpy and free energy where a greater negative value of free energy suggests spontaneous binding and interactions [44]. Here, ^MSal-OPD-Sal^MH₂, BzA-OPD-BzAH₂, HNP-BD-HNPH₂, ^MSal-HD-Sal^MH₂ and BzA-HD-BzAH₂ showed greater values of free energy (-1260.4492, 1264.8189, -1264.8264, -1265.1956 and -1269.5664 Hartree, respectively) compared to others. In drug design, improved dipole moment could illustrate their binding mode(s) within a specific target protein [45], better polar nature and hydrogen bond formation. ^MSal-HD-Sal^MH₂, BzA-OPD-BzAH₂ and ^MSal-OPD-Sal^MH₂ showed the highest dipole moment values of 3.3384, 4.4183 and 4.4699 Debye, respectively.

Table 1 Molecular formula (MF), molecular weight (MW), enthalpy, free energy (Hartree) and dipole moment (Debye) of ligands.

Series	Ligands & code	MF	MW	Enthalpy	Free energy	Dipole moment
Series 1	^M Sal-ED-Sal ^M (1)	C ₁₈ H ₂₀ N ₂ O ₄	328	-1107.9553	-1108.0361	0.0003
	HNP-ED-HNPH ₂ (2)	C ₂₄ H ₂₀ N ₂ O ₂	368	-1186.1650	-1186.2465	0.0001
	BzA-ED-BzAH ₂ (3)	C ₂₂ H ₂₄ N ₂ O ₂	348	-1112.3223	-1112.4105	4.2543
Series 2	^M Sal-1,2-PD-Sal ^M (4)	C ₁₉ H ₂₂ N ₂ O ₄	342	-1147.2420	-1147.3253	0.6851
	HNP-1,2-PD-HNPH ₂ (5)	C ₂₅ H ₂₂ N ₂ O ₂	382	-1225.4555	-1225.5399	0.3480
	BzA-1,2-PD-BzAH ₂ (6)	C ₂₃ H ₂₆ N ₂ O ₂	362	-1151.6102	-1151.7010	2.9888
Series 3	^M Sal-1,3-PD-Sal ^M (7)	C ₁₉ H ₂₂ N ₂ O ₄	342	-1147.2422	-1147.3265	1.7340
	HNP-1,3-PD-HNPH ₂ (8)	C ₂₅ H ₂₂ N ₂ O ₂	382	-1225.4520	-1225.5366	0.6322
	BzA-1,3-PD-BzAH ₂ (9)	C ₂₃ H ₂₆ N ₂ O ₂	362	-1151.6090	-1151.7002	0.5830
Series 4	^M Sal-BD-Sal ^M (10)	C ₂₀ H ₂₄ N ₂ O ₄	356	-1186.5285	-1186.6157	3.4186
	HNP-BD-HNPH ₂ (11)	C ₂₆ H ₂₄ N ₂ O ₂	396	-1264.7383	-1264.8264	3.4959
	BzA-BD-BzAH ₂ (12)	C ₂₄ H ₂₈ N ₂ O ₂	376	-1190.8962	-1190.9909	1.5010
Series 5	^M Sal-HD-Sal ^M (13)	C ₂₂ H ₂₈ N ₂ O ₄	384	-1265.1008	-1265.1956	3.3384
	HNP-HD-HNPH ₂ (14)	C ₂₈ H ₂₈ N ₂ O ₂	424	-1114.6858	-1114.7759	1.0176
	BzA-HD-BzAH ₂ (15)	C ₂₆ H ₃₂ N ₂ O ₂	436	-1269.4678	-1269.5664	1.7066
Series 6	^M Sal-OPD-Sal ^M (16)	C ₂₂ H ₂₀ N ₂ O ₄	376	-1260.3648	-1260.4492	4.4699
	HNP-OPD-HNPH ₂ (17)	C ₂₈ H ₂₀ N ₂ O ₂	416	-1338.5745	-1338.6601	3.9435
	BzA-OPD-BzAH ₂ (18)	C ₂₆ H ₂₄ N ₂ O ₂	396	-1264.7280	-1264.8189	4.4183

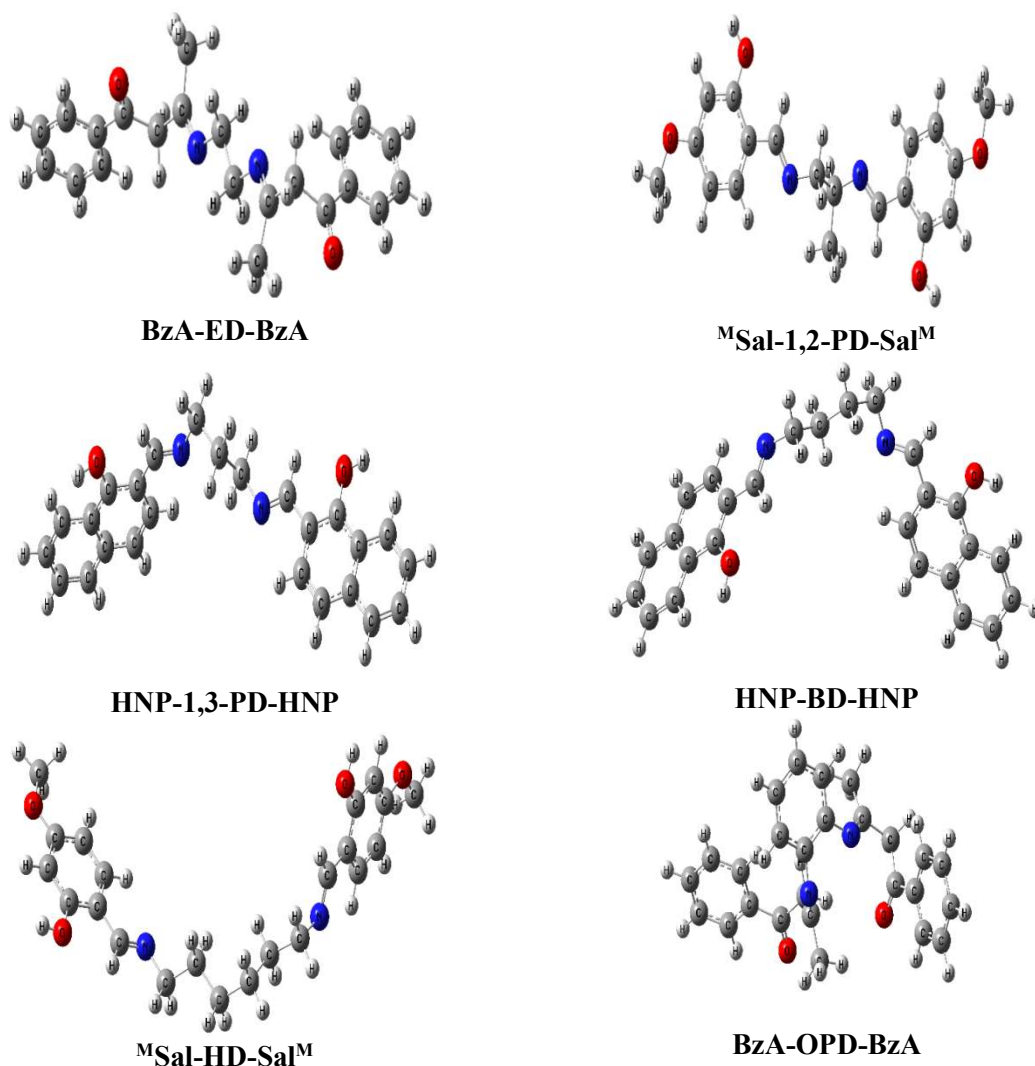


Figure 2. Optimized structure of some representative Schiff Bases by DFT

3.2 Frontier molecular orbital analysis

Frontier molecular orbitals (FMOs) consist of the highest occupied molecular orbital (HOMO) and lowest unoccupied molecular orbital (LUMO) is related to structure-activity relationships [46]. Frontier molecular orbitals and related energies of all ligands (1-18) are presented in Table 2. The electron transfers from ground state HOMO to the first excited energy state LUMO as described by one electron excitation [47]. HOMO is an electron donor as it is occupied, whereas LUMO is an electron acceptor due to an unoccupied energy orbital [48]. These orbitals control the binding mode(s) and interactions between ligands with the receptor protein. The HOMO-LUMO energy gap is also a key tool for kinetic stability and chemical reactivity [49], where a small gap insists on greater chemical reactivity. The FMOs energy analysis result revealed that ^MSal-HD-Sal^MH₂ (Figure 3) has the lowest HOMO-LUMO gap (3.4374 eV) and the highest softness (0.5818 eV) with a chemical potential (-6.6951 eV).

Table 2. Energy of HOMO-LUMO (eV), gap, hardness, softness and chemical potential of investigated ligands

Ligands	ν HOMO	ν LUMO	Gap	Hardness	Softness	Chemical potential
^M Sal-ED-Sal ^M (1)	-5.5430	-0.7962	4.7468	2.3734	0.4213	-3.1696
HNP-ED-HNPH ₂ (2)	-5.5239	-1.3461	4.1778	2.0889	0.4787	-3.4350
BzA-ED-BzAH ₂ (3)	-6.4711	-1.6093	4.8618	2.4309	0.4114	-4.0502
^M Sal-1,2-PD-Sal ^M (4)	-5.5196	-0.7804	4.7392	2.3696	0.4220	-3.1500
HNP-1,2-PD-HNPH ₂ (5)	-5.5158	-1.3459	4.1699	2.0850	0.4796	-3.4309
BzA-1,2-PD-BzAH ₂ (6)	-6.3245	-1.6596	4.6649	2.3325	0.4287	-3.9921
^M Sal-1,3-PD-Sal ^M (7)	-5.5217	-0.7750	4.7467	2.3734	0.4213	-3.1484
HNP-1,3-PD-HNPH ₂ (8)	-5.4845	-1.3260	4.1585	2.0793	0.4809	-3.4053
BzA-1,3-PD-BzAH ₂ (9)	-6.4820	-1.6721	4.8099	2.4050	0.4158	-4.0771
^M Sal-BD-Sal ^M (10)	-5.5650	-0.7499	4.8151	2.4076	0.4154	-3.1575
HNP-BD-HNPH ₂ (11)	-5.4972	-1.3181	4.1791	2.0896	0.4786	-3.4077
BzA-BD-BzAH ₂ (12)	-6.5354	-1.6270	4.9084	2.4542	0.4075	-4.0812
^M Sal-HD-Sal ^M (13)	-8.4138	-4.9764	3.4374	1.7187	0.5818	-6.6951
HNP-HD-HNPH ₂ (14)	-5.8973	-0.6596	5.2377	2.6189	0.3818	-3.2785
BzA-HD-BzAH ₂ (15)	-9.2443	-5.4338	3.8105	1.9053	0.5249	-7.3391
^M Sal-OPD-Sal ^M (16)	-5.0502	-1.1197	3.9305	1.9653	0.5088	-3.0850
HNP-OPD-HNPH ₂ (17)	-5.1955	-1.5584	3.6371	1.8186	0.5499	-3.3770
BzA-OPD-BzAH ₂ (18)	-5.5323	-1.5715	3.9608	1.9804	0.5049	-3.5519

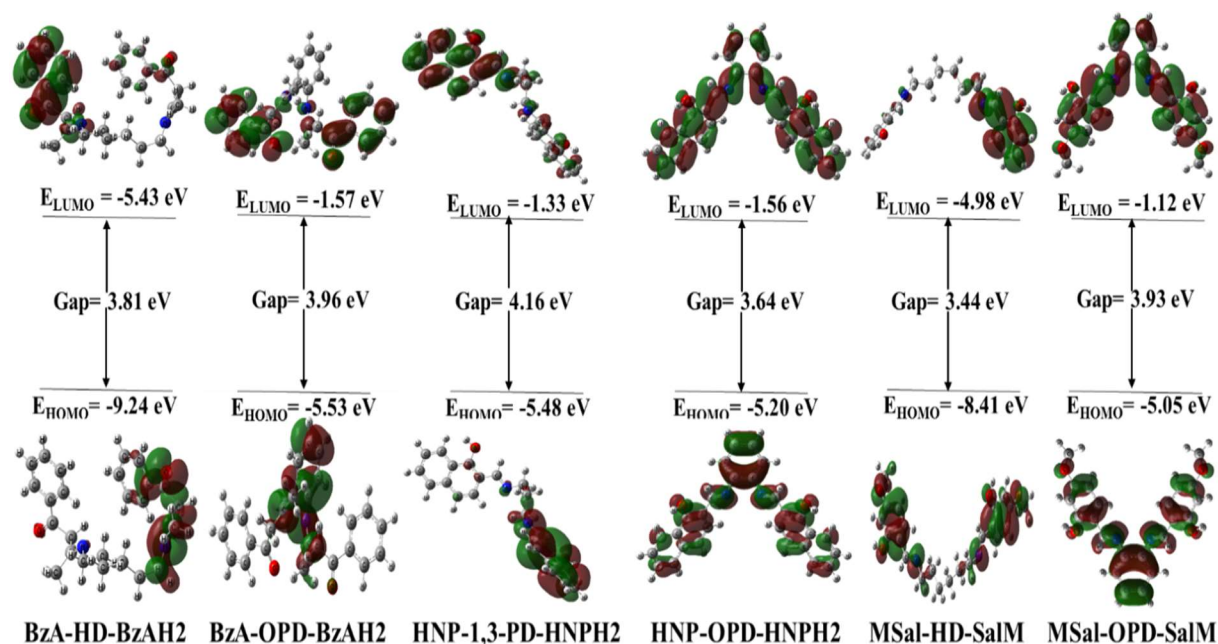


Figure 3. Frontier molecular orbital features of BzA-HD-BzA, BzA-OPD-BzA, HNP-1,3-PD-HNP, HNP-OPD-HNP, ^MSal-HD-Sal^M and ^MSal-OPD-Sal^M

3.3 Molecular electrostatic potential (MEP)

To validate the evidence about the reactive sites for the electrophilic and nucleophilic attack, it is important to calculate the molecular electrostatic potential. Although it gives an indication of molecular size and shape of the positive, negative and zero potential in terms of color grading, it also helps to predict hydrogen bonding interaction and biological recognition process [50]. The MEP of ligands (**1-18**) is calculated by the same level of theory. In the MEP, the maximum negative region is a favorable site for electrophilic attack (indicated in red) and the maximum positive region is a favorable site for nucleophilic attack (indicated in blue). The area in green is considered as zero potential areas. It is observed that the orientation of $-ve$, $+ve$ and zero potential as well as molecular size and shape varied because of the atoms and their electronic nature present in the molecule. From MEP, it is found that HNP-OPD-HNP showed the maximum negative potentiality (-0.2508 a.u.) and the maximum positive potentiality ($+0.1645$ a.u.) as shown in Figure 4.

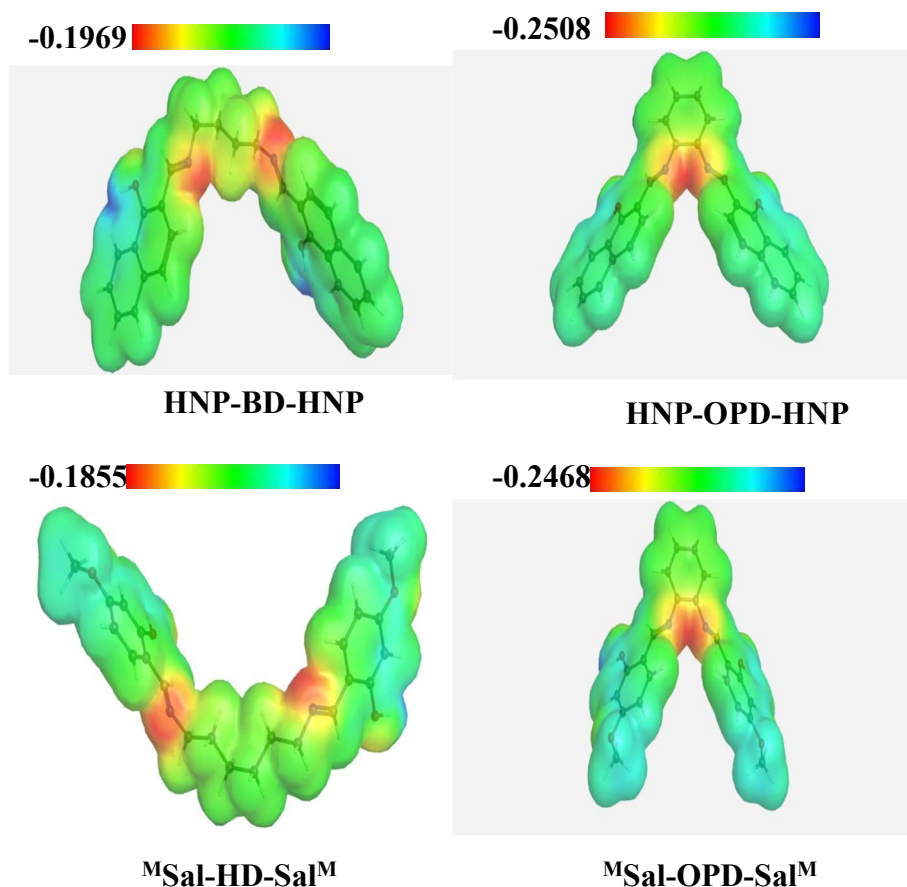


Figure 4. Molecular electrostatic potential of HNP-BD-HNP, HNP-OPD-HNP, ^MSal-HD-Sal^M and ^MSal-OPD-Sal^M

3.4 Molecular docking studies

Molecular docking studies were performed to predict the binding properties of ligands (1-18) against the SARS-CoV-2 Mpro (6LU7). The docking results with SARS-CoV-2 Mpro were compared to some FDA-approved antiviral drugs like chloroquine, hydroxychloroquine and remdesivir, which were used as control. The binding affinity of ligands (1-18) ranged from -5.8 to -8.2 kcal/mol as depicted in Table 3.

Table 3. Binding affinity and nonbonding interaction of ligands with SARS Cov-2 Mpro

Ligands	Binding affinity (kcal/mol)	Contact residues, Interaction type, distance (Å)
^M Sal-ED-Sal ^M (1)	-6.4	Gly120, H (2.3); Gln69, H (2.7); Gly15, H (2.4); Gln19, H (2.5); Met17, C (2.6); Gly120, C (2.21); Lys97, PC (4.6); Ala70, PS (2.8); Trp31, Pp (5.7)
HNP-ED-HNPH ₂ (2)	-7.9	Leu287, H (2.21); Asp289, C (2.5); Asp289, AC (4.2); Lys5, PiC (4.5), Glu290, PiA (4.6); Leu287, PA (4.3); Lys137, PA (4.9)
BzA-ED-BzAH ₂ (3)	-6.3	Gln110, H (2.8); Gln110, H (2.); Gln110, H (2.5); Phe294, Pp (3.8)
^M Sal-1,2-PD-Sal ^M (4)	-6.6	Asp289, H (2.3); Leu287, H(2.4); Leu287, H(1.9); Glu288, H(2.0); Lys5, H(2.1); Leu287, H (2.3); Asp289, AC (4.7); Asp289, PiA(4.7); Glu290, PiA (3.9); Leu287, PA(4.8); Lys137, PA (5.4)
HNP-1,2-PD-HNPH ₂ (5)	-8.2	Gln110, H (2.2); Phe294, Pp(3.8); His246, PpTs(4.7)
BzA-1,2-PD-BzAH ₂ (6)	-6.9	Gln110, H(2.1); Phe294, H(2.4); Phe294, PC(4.8); Pro293, Aps(4.2); Val104, PA(5.4); Ile106, PA(5.4); Pro252, PA(5.3); Val297, PA(4.6)
^M Sal-1,3-PD-Sal ^M (7)	-6.4	Gly120, H(2.1); Met17, H(2.0); Gly120, H(2.7); Gly15, H(2.2); Glu14, C(2.5); Gly120, C(2.7); Ala70, C (2.1); Lys97, C(2.7); Ala70, PiC(4.6); Gly71, Aps(4.2); Ala70, PA(4.1)
HNP-1,3-PD-HNPH ₂ (8)	-7.8	Tyr237, H(2.5); Thr199, C(2.9); Asn238, C(2.5); Asp197, AC(4.6); Asp289, AC(5.0); Asp289, PiA(3.2); Tyr239, PpTs (5.4); Leu272, PA(4.8); Leu287, PA(5.5)
BzA-1,3-PD-BzAH ₂ (9)	-6.3	Tyr237, H(2.6); Arg131, H (2.6); Thr199, H(1.9); Tyr239, H(2.3); Thr199, C(3.0); Leu287, PA (4.3)
^M Sal-BD-Sal ^M (10)	-5.8	Leu141, H(2.4); Leu141, C(2.5); Tyr54, C(2.8); Asp187, C(2.0); Gly143, Pdh(3.9); Cys145, Ps(5.7); Met49, PA(4.7)
HNP-BD-HNPH ₂ (11)	-6.4	Phe294, Pp(3.9); Phe294, Pp(3.7)
BzA-BD-BzAH ₂ (12)	-5.8	Gln110, H(2.2); Gln110, H(2.9); Gln110, H(2.9); Phe294, Pp(3.9)

Ligands	Binding affinity (kcal/mol)	Contact residues, Interaction type, distance (Å)
^M Sal-HD-Sal ^M (13)	-5.8	Gln189, H(2.20); Cys145, H(2.9); Leu141, C(2.5); His163, C(2.7); Asp187, C(2.7); His41, Ppts(4.8); Met49, PA(5.2); Met165, PA(5.4); Cys145, PA(5.3)
HNP-HD-HNPH ₂ (14)	-6.3	Gln110, H(2.4); Gln110, C(3.0); Phe294, Pp(3.9); Phe294, Pp(3.9)
BzA-HD-BzAH ₂ (15)	-6.0	Thr199, H(1.9); Arg131, H(2.5); Tyr239, H(2.4); Asp197, C(3.0); Thr199, C(2.9); Leu287, PA(4.2); Leu286, PA(4.6); Asp197, AC(4.7); Asp289, AC(5.4)
^M Sal-OPD-Sal ^M (16)	-7.1	Gln189, H(3.0); His41, C(2.7); Thr26, C(2.5); Asn142, C(2.6), Phe140, C(2.9), Gly143, C(2.9), His41, PiC(4.5), Met49, PA(4.9), Met165, PA(5.3); Cys145, PA(5.0)
HNP-OPD-HNPH ₂ (17)	-8.2	Glu166, AC(4.1); Glu166, PiA(4.0), His41, PpTs(4.9); Met165, PA(4.8); Pro168, PA(5.0)
BzA-OPD-BzAH ₂ (18)	-6.7	Asp153, SB; H(2.9); Gln110, H(2.8); Asn151, H(2.6); Phe294, Pp(3.9), Val104, PA(5.3), Ile106, PA(4.8)
HCQ	-5.8	Tyr154, H(2.5); Gln110, H(2.8); Thr111, H(2.9); Asp153, C(2.4); Gln110, C(2.6); Thr111, C(2.2)

H: Conventional hydrogen bond, C: Carbon hydrogen bond, A: Alkyl, PA: Pi-Alkyl, Pp: Pi-pi stacked, AC: Attractive charge, PpTs: Pi-pi T-shaped, Aps: Amide Pi-Stacked, SB: Salt bridge, PiA: Pi-Anion, PiC: Pi-Cation, Pdh: Pi-donor hydrogen bond

Figure 5 shows the docked confirmation of HNP-OPD-HNPH₂, ^MSal-BD-Sal^MH₂, ^MSal-HD-Sal^MH₂ and ^MSal-OPD-Sal^MH₂ at the inhibition binding site of receptor protein SARS-CoV-2 Mpro. Most of the ligands did not demonstrate any significant interactions with the Cys-His catalytic dyad of 6LU7 [51] despite having increased binding affinity such as BzA-ED-BzAH₂ (-6.3 kcal/mol), BzA-1,2-PD-BzAH₂ (-6.9 kcal/mol), BzA-1,3-PD-BzAH₂ (-6.3 kcal/mol), BzA-BD-BzAH₂ (-5.8 kcal/mol), BzA-HD-BzAH₂ (-6.0 kcal/mol), BzA-OPD-BzAH₂ (-6.7 kcal/mol), HNP-ED-HNPH₂ (-7.9 kcal/mol), HNP-1,2-PD-HNPH₂ (-8.2 kcal/mol), HNP-1,3-PD-HNPH₂ (-7.8 kcal/mol), HNP-BD-HNPH₂ (-6.4 kcal/mol), HNP-HD-HNPH₂ (-6.3 kcal/mol), ^MSal-ED-Sal^MH₂ (6.4 kcal/mol), ^MSal-1,2-PD-Sal^MH₂ (6.6 kcal/mol) and ^MSal-1,3-PD-Sal^MH₂ (6.4 kcal/mol). ^MSal-HD-Sal^MH₂ and ^MSal-OPD-Sal^MH₂ bind with both of the Cys-His catalytic dyad containing increased binding affinity of -5.8 and -7.1 kcal/mol respectively but ^MSal-BD-Sal^MH₂ (-5.8 kcal/mol) and HNP-OPD-HNPH₂ (-8.2 kcal/mol) bind with one of those catalytic dyads. Binding affinity with SARS-CoV-2 Mpro of some FDA-approved drugs chloroquine [10], hydroxychloroquine [10] and remdesivir [12] was reported as -4.3 kcal/mol, -5.2 kcal/mol and -5.5 kcal/mol, respectively. In our investigation, hydroxylchloroquine (HCQ) was docked as standard with the same receptor protein, SARS-CoV-2 main protease (6LU7) to compare the results.

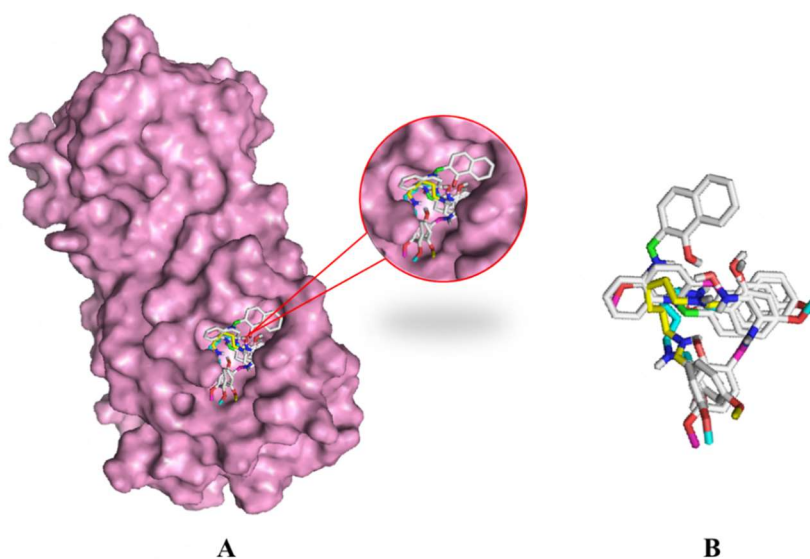


Figure 5. (A) Docked confirmation of selected Schiff bases at inhibition binding site of receptor protein SARS CoV-2 Mpro, (B) Superimposed view of them after docking simulation

3.5 Structural activity relationship of binding affinity

Schiff bases derived from diamine and aldehyde/ketone are formulated with their structural backbone as $R-C=N-(CH_2)_n-N=C-R$. It consists of a central diamine linkage and two similar terminal linkages of aldehyde/ketone. Depending upon the diamine linkage, Schiff bases are grouped into six series (Table 1). Both linkages have effects on the binding affinity that are summarized below.

Effect of central linkage: It is noted that binding affinity of Schiff bases decreases with the increase of the number of carbon in the aliphatic chain (elongation of chain) in amines. Schiff bases of OPD (orthophenylenediamine), an aromatic diamine, showed the highest bonding affinity. Schiff bases of 1,2-pn (1,2-propanediamine) have greater binding affinity than those from en (ethylenediamine) though both contain the same number of carbon ($n=2$). It is because of the presence of a CH_3 - group in central linkage as a branch exhibiting carbon hydrogen nonbonding interaction with protein. *Effect of terminal linkage:* Binding affinity Schiff bases of each series follow the sequence $HNP > Sal > BzA$ being attached as terminal linkage.

3.6 PASS prediction

Selected PASS results were designated as Pa and Pi forms. The compounds showing more Pa value than Pi as presented in Table 4 are the only constituents considered as possible for a particular pharmacological activity. Ligands, BzA-ED-BzAH₂ and BzA-1,2-PD-BzAH₂ having Pa values 0.637 and 0.694, respectively exhibited their anti-neurotic activity. It is remarkable that Schiff bases prepared from BzA did not show an antioxidant property. The remaining showed $0.133 < Pa < 0.237$ in PASS analysis for antioxidant activity, where the compound ^MSal-HD-Sal^MH₂ showed the highest antioxidant property. PASS prediction of the Schiff bases showed $0.363 < Pa < 0.795$, $0.292 < Pa < 0.484$ and $0.172 < Pa < 0.313$ for anti-inflammatory, intestinal anti-inflammatory, and ophthalmic anti-inflammatory activities respectively indicating them as more potent anti-inflammatory agents, except

BzA-1,3-PD-BzAH₂, which are intestinal anti-inflammatory active. 0.177<Pa<0.447 for antiviral, 0.245<Pa<0.403 for influenza antiviral and 0.125<Pa<0.288 for HIV antiviral activity were found from PASS analysis. All Schiff bases were found to be influenza antiviral active except ^MSal-1,3-PD-Sal^MH₂. 0.200<Pa<0.399 was found for the antibacterial activity of Schiff bases except those prepared from BzA. A few of the tested Schiff bases showed poor ophthalmic antibacterial activity. All tested Schiff bases were found to be antifungal active with 0.208<Pa<0.379 as found from PASS analysis. It is indicated that Schiff bases are stronger antiviral than antibacterial or antifungal agents. Most of the Schiff bases proved to be anticarcinogenic as PASS prediction showed 0.180<Pa<0.299. HNP-OPD-HNPH₂ and ^MSal-OPD-Sal^MH₂ were the strongest antituberculosis with Pa values 0.662 and 0.671, respectively.

Table 4. Comparison of selected biological activities (Pa) of Schiff bases predicted by PASS analysis

SB	Antioxidant	Anti-inflammatory	Anti-inflammatory (intestinal)	Anti-inflame (opt)	Antiviral	Antiviral (influenza)	Antiviral (HIV)	Antibacterial	Antibacterial (opt)	Antifungal	Anti-carcinogenic	Anti-tuberculosis
1	0.226	0.405	0.435	0.305	0.18	0.259	0.129	0.227	0.134	0.29	0.22	0.359
2	0.156	0.363	0.324	0.263	0.258	0.245	0.189	0.236	0.13	0.257	0.185	0.368
3		0.795	0.424	0.292	0.335	0.302	0.288		0.16	0.218		0.244
4	0.191		0.396	0.273		0.26		0.301		0.36	0.203	0.342
5	0.133		0.292		0.188	0.246	0.136	0.309		0.346		
6		0.67	0.4	0.276	0.307	0.343	0.25			0.251		0.263
7	0.215		0.417	0.313		0.282		0.219		0.26	0.277	0.296
8	0.155		0.31		0.181	0.267	0.125	0.227		0.247	0.299	0.305
9		0.65		0.3	0.262	0.332	0.21		0.0149	0.208	0.198	
10	0.215		0.417	0.313		0.282		0.219		0.26	0.277	0.296
11	0.167		0.31		0.177	0.306		0.232	0.131	0.266	0.221	0.357
12		0.663	0.401	0.275	0.256	0.388	0.204		0.167	0.229	0.192	
13	0.237		0.435			0.34		0.226		0.295	0.27	0.384
14	0.172		0.325		0.172	0.319		0.235	0.135	0.283	0.223	0.357
15		0.662	0.419	0.172	0.447	0.403	0.195		0.172	0.248		
16	0.212		0.484	0.31				0.384		0.379		0.662
17	0.153		0.363	0.268		0.252		0.399		0.369	0.18	0.671
18			0.472	0.3	0.27	0.317	0.23	0.2	0.148	0.306		0.341

^MSal: p-methoxy-salicylaldehyde, HNP: 2-hydroxy-1-naphthaldehyde; BzA: benzoylacetoacetate; ED: ethanediamine; PD: propanediamine; BD: 1,4-butanediamine; HD: 1,6-hexanediamine; OPD: ortho-phenyldiamine

3.7 ADMET studies

The results from AdmetSAR calculation of ligands (1-18) are shown in Table 5. All ligands exhibited positive responses for the blood-brain barrier (BBB). Minimum BBB $+(0.5232)$ for HNP-BD-HNPH₂, and maximum $+(0.9660)$ for ligand BzA-HD-BzAH₂ were found. All ligands showed a positive response for human intestinal absorption with a minimum $+(0.5132)$ for HNP-BD-HNPH₂ and a maximum $+(0.9810)$ for BzA-1,2-PD-BzAH₂. All ligands were found to be non-carcinogenic with values of 0.6015 to 0.8546 and showed type III acute oral toxicity. Most of the ligands were P-glycoprotein non-inhibitor except BzA-1,3-PD-BzAH₂, BzA-BD-BzAH₂, BzA-HD-BzAH₂. Some ligands showed strong inhibitory features for human ether-a-go-go-related gene (hERG).

Table 5 Selected pharmacokinetic parameters of ligands

Ligands	Blood brain barrier	Human intestinal absorption	P-glycoprotein inhibitor	hERG	Carcinogen	Rat acute toxicity (LD ₅₀) mol/kg	Acute oral toxicity
1	$+(0.9403)$	$+(0.9711)$	NI(0.8475)	WI(0.5680)	NC(0.7906)	2.2896	III
2	$+(0.7345)$	$+(0.7397)$	NI(0.8726)	SI(0.6291)	NC(0.7863)	2.2777	III
3	$+(0.6321)$	$+(0.9077)$	NI(0.7786)	SI(0.7000)	NC(0.7609)	2.2733	III
4	$+(0.9030)$	$+(0.8658)$	NI(0.8134)	WI(0.8929)	NC(0.7511)	2.3277	III
5	$+(0.6703)$	$+(0.7848)$	NI(0.7947)	WI(0.7818)	NC(0.7621)	2.2730	III
6	$+(0.6985)$	$+(0.9810)$	NI(0.7850)	WI(0.5704)	NC(0.6890)	2.3711	III
7	$+(0.8874)$	$+(0.8235)$	NI(0.7506)	WI(0.7332)	NC(0.8246)	2.2438	III
8	$+(0.6394)$	$+(0.7227)$	NI(0.7511)	WI(0.5552)	NC(0.8266)	2.2828	III
9	$+(0.6288)$	$+(0.9714)$	I(0.5911)	SI(0.5160)	NC(0.8328)	2.1269	III
10	$+(0.8157)$	$+(0.9200)$	NI(0.8066)	WI(0.6100)	NC(0.8546)	2.3039	III
11	$+(0.5232)$	$+(0.5132)$	NI(0.8369)	SI(0.5862)	NC(0.8544)	2.3119	III
12	$+(0.8169)$	$+(0.9653)$	I(0.5110)	SI(0.5915)	NC(0.8465)	2.2005	III
13	$+(0.6262)$	$+(0.5219)$	NI(0.6644)	WI(0.5206)	NC(0.7939)	2.3494	III
14	$+(0.6626)$	$+(0.9282)$	NI(0.7147)	SI(0.6178)	NC(0.8182)	2.2838	III
15	$+(0.9660)$	$+(0.9605)$	I(0.7629)	WI(0.7092)	NC(0.6451)	2.0827	III
16	$+(0.7929)$	$+(0.9393)$	NI(0.8261)	WI(0.8698)	NC(0.8404)	2.2433	III
17	$+(0.6386)$	$+(0.5535)$	NI(0.8637)	WI(0.7520)	NC(0.8419)	2.2938	III
18	$+(0.7561)$	$+(0.7822)$	NI(0.9277)	WI(0.7086)	NC(0.6015)	2.3249	III
HC Q	$+(0.5602)$	$+(0.9892)$	NI(0.7297)	WI(0.6798)	NC(0.8370)	2.6348	III

NI: Non-inhibitor, WI: Weak-inhibitor, NC: Non-carcinogenic

4. Discussion

Schiff bases, ^MSal-OPD-Sal^MH₂, BzA-OPD-BzAH₂, HNP-BD-HNPH₂, ^MSal-HD-Sal^MH₂ and BzA-HD-BzAH₂ having greater free energy are suggested energetically and configurationally more stable [27-29]. BzA-OPD-BzAH₂ and ^MSal-OPD-Sal^MH₂ showed comparatively highest dipole moment which contributed greater binding affinity and non-bonding interactions. The lowest HOMO-LUMO gap and highest softness of ^MSal-HD-Sal^MH₂ may be contributed to its better chemical reactivity and polarizability. Both negative and positive potentiality of HNP-OPD-HNPH₂ were found to be maximum from MEP which indicated that it would be attracted by either electrophile or nucleophile easily [26].

HNP-ED-HNPH₂ (-7.9 kcal/mol), HNP-1,2-PD-HNPH₂ (-8.2 kcal/mol), HNP-1,3-PD-HNPH₂, HNP-OPD-HNPH₂ showed their increased binding affinity with SARS-CoV-2 Mpro (Figure 6). The essential amino acids residues for the interaction with ligands are recognized as Leu267/272, Asp289/238, Lys5/137, Glu116/290, Gln110, Phe294, His41/246, Met164, Pro168, Tyr239/237, Thr199, Asn238 etc. [52, 53]. Besides hydrogen bonding, electrostatic and hydrophobic non-covalent bond (carbon hydrogen bond, alkyl, Pi-Alkyl and Pi-pi stacked) were observed which were responsible for their highest binding affinity (Figures 7 and 8). The molecular docking results revealed that the effective interactions between these four ligands with 6LU7 were obtained on the electronegative atoms and it could be attributed to the presence of lone pair of electrons. In addition, the π - π T-shaped could be another hydrophobic interaction of ligands with the receptor. Hydrogen bond surface shows that amino acid residues like Pro168, Glu166, His41, Leu141, Gly143, His163, Asn142 and Thr26 help in creating strong donor regions and residues like Met165, Met49, Cys145, asp187, Gln189 and Phe140 help in creating strong acceptor regions on drug-protein interaction surface[26].

^MSal-HD-Sal^MH₂, ^MSal-OPD-Sal^MH₂ and ^MSal-BD-Sal^MH₂ also showed better binding energy along with strong hydrogen bonds with other residues and observed that they are capable to bind with both of the Cys-His catalytic dyad or one of them (His41 and Cys145) [51]. They might be used as better SARS-CoV-2 Mpro inhibitors due to their comparable binding affinity with SARS-CoV-2 Mpro to FDA-approved drugs chloroquine [10], hydroxychloroquine [10] and remdesivir [12]. Besides hydrogen bonds, different non-covalent interactions like hydrophobic interactions occurred with amino acid residues Gln189, Cys145, Leu141, His163 and Asp187 in a distance of 2.24, 2.97, 2.45, 2.71 and 2.66 Å for ^MSal-HD-Sal^MH₂ whereas Gln189, His41, Thr26, Asn142, Phe140 and Gly143 with a distance of 3.0458, 2.6876, 2.5314, 2.6125, 2.9886 and 2.9417 Å for ^MSal-OPD-Sal^MH₂ [54]. In ^MSal-BD-Sal^MH₂, four hydrogen bonds were observed including some hydrophobic interactions.

In this investigation, the binding affinity -5.8 kcal/mol of standard (HCQ) was found which was comparable to or less than our tested Schiff base ligands. In the case of HCQ, hydrogen bonding and carbon-hydrogen bond interactions with Tyr154, Gln 110, Thr 111, and Asp 153 amino acid residues of the protein were identified. The results of molecular docking revealed that almost all ligands had the highest binding affinity with the receptor protein. Hence, it predicts that they might serve as better inhibitor than standard (HCQ) [55].

Prediction of activity spectra for substances (PASS) was applied for the assessment of biological activity. Out of the >250 estimated spectrum of biological activities, special attention has been given to the results predicting the probability of antineurotic, antioxidant, anti-inflammatory, anticarcinogenic antituberculosis, antifungal, antiviral and antibacterial activities of Schiff bases (Table 4).

All ligands exhibited positive responses for blood-brain barrier (BBB) and human intestinal absorption. Ligands are found to be non-carcinogenic and show type III acute oral toxicity, suggesting harmless for oral administration [56]. Most of the ligands except BzA-1,3-PD-BzAH₂, BzA-BD-BzAH₂ and BzA-HD-BzAH₂ are P-glycoprotein non-inhibitor, where their inhibition can interrupt the absorption, permeability and retention of the drugs [57]. Furthermore, some ligands show strong inhibitory features for human ether-a-go-go-related gene (hERG), whereas other ligands are indicating weak that can lead to long QT syndrome [58]. Still, further study of this aspect is essential.

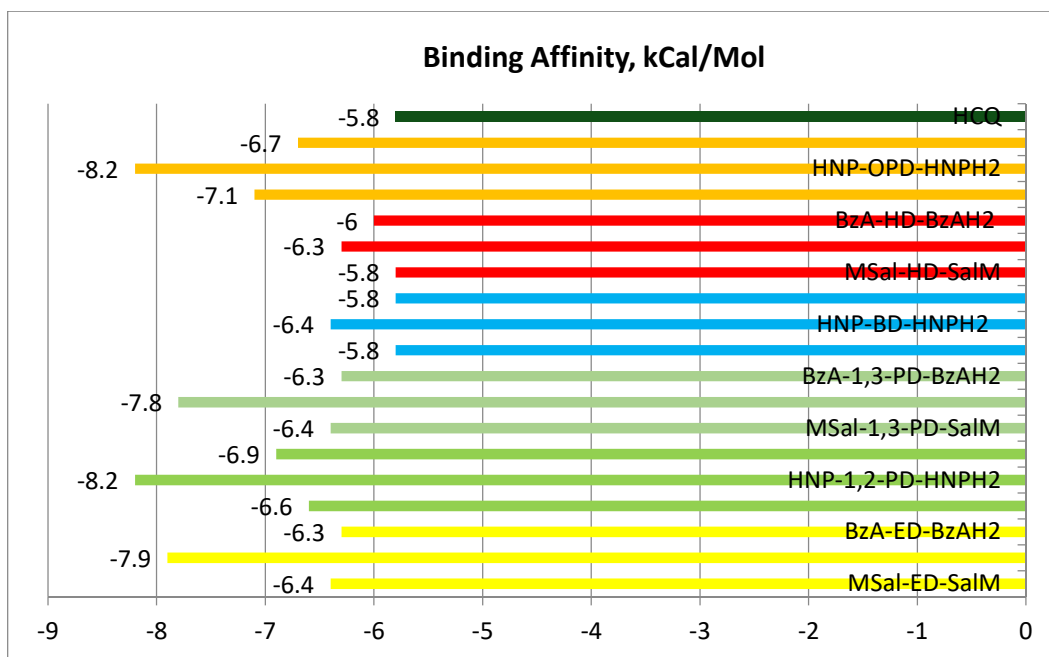


Figure 6. Comparison of binding affinity of Schiff bases with hydroxychloroquine (HCQ) against SARS CoV-2 Mpro

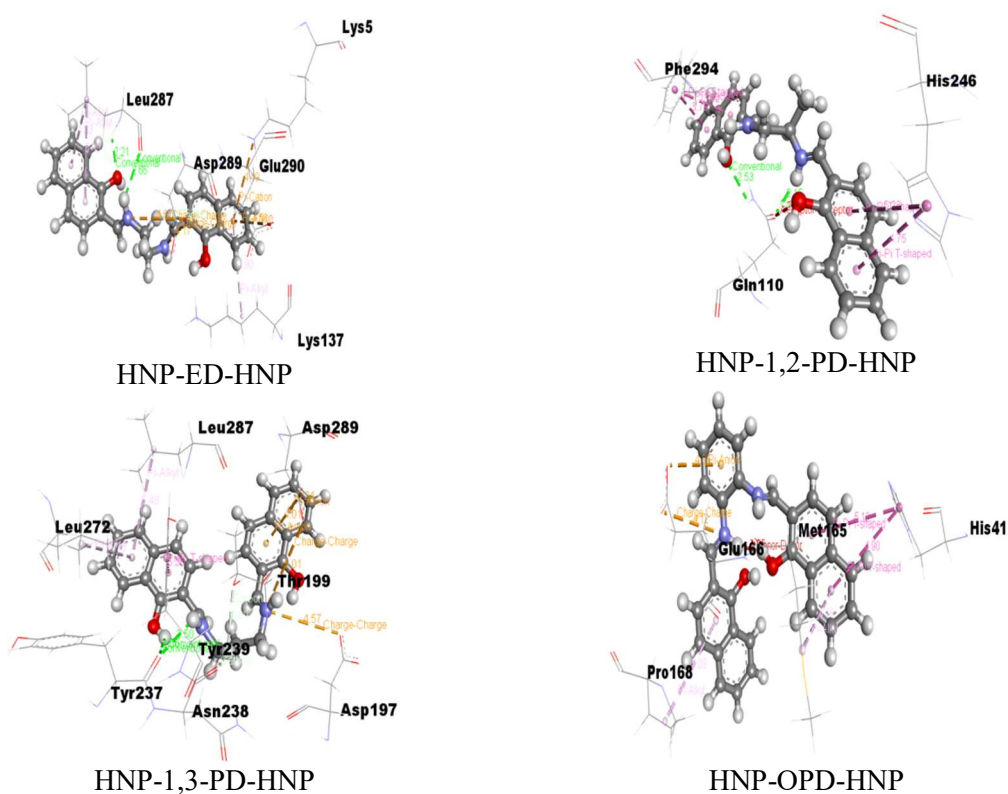


Figure 7. Non-bonding interactions of selected Schiff bases with receptor protein SARS Cov-2 Mpro generated by Discovery Studio

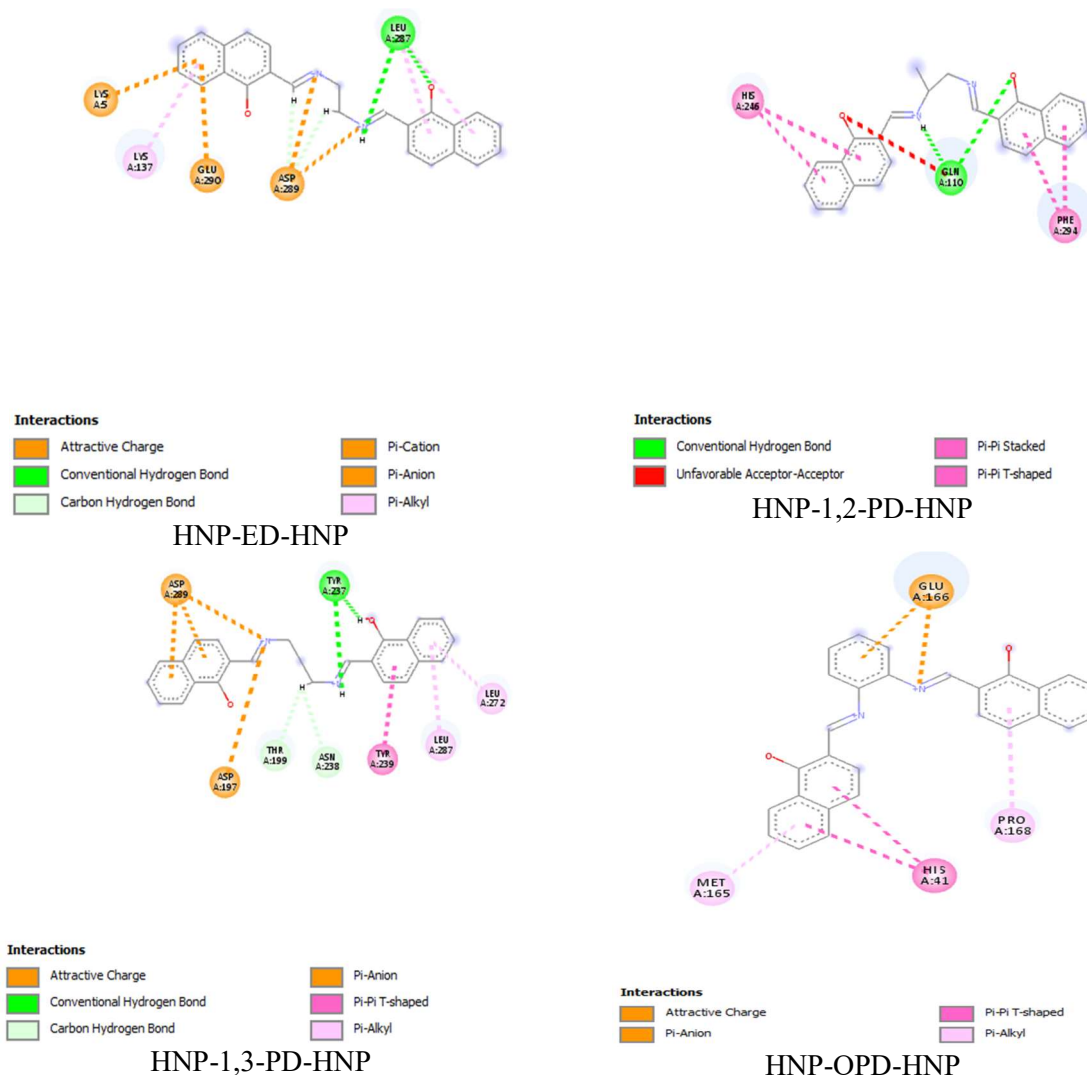


Figure 8. 2D form of non-bonding interactions of selected Schiff bases with receptor protein

5. Conclusion

The DFT calculation revealed that all the ligands were thermally stable and had a small HOMO-LUMO gap of ${}^M\text{Sal-HD-Sal}^M\text{H}_2$ with the highest softness, the polarizability and chemical activities were enhanced. The docking results predicted that HNP-ED-HNPH₂, HNP-1,2-PD-HNPH₂, HNP-1,3-PD-HNPH₂, ${}^M\text{Sal-OPD-Sal}^M\text{H}_2$ and HNP-OPD-HNPH₂ had improved binding affinity (-7.9, -8.2, -7.8, -7.1 and -8.2 kcal/mol, respectively) against 6LU7. Interestingly most of the Schiff bases showed greater binding affinity than those FDA-approved drugs, chloroquine, hydroxychloroquine and remdesivir. Considering this *in silico* prediction, HNP-ED-HNPH₂, HNP-1,2-PD-HNPH₂, HNP-1,3-PD-HNPH₂, ${}^M\text{Sal-OPD-Sal}^M\text{H}_2$ and HNP-OPD-HNPH₂ were found as the promising inhibitors against 6LU7. Therefore, to establish their activity as COVID-19 inhibitors, solid experimental evidence of *in vitro* and *in vivo* studies is required. PASS analysis indicated that Schiff bases are stronger antiviral than antibacterial or antifungal agents.

List of Abbreviations: COVID-19: coronavirus disease 2019; DFT: density functional theory; SARS-CoV-2: severe acute respiratory syndrome coronavirus-2; ^MSal: p-methoxy-salicylaldehyde, HNP: 2-hydroxy-1-naphthaldehyde; BzA: benzoylacetone; ED: ethanediamine; PD: propanediamine; BD: 1,4-butanediamine; HD: 1,6-hexanediamine; OPD: ortho-phenyldiamine; Mpro: main protease; FDA: food and drug administration

References

- [1] Lai, C. C., Shih, T. P., Ko, W. C., Tang, H. J., & Hsueh, P. R. (2020). Severe acute respiratory syndrome coronavirus 2 (SARS-CoV-2) and coronavirus disease-2019 (COVID-19): The epidemic and the challenges. *International journal of antimicrobial agents*, 55(3), 105924. <https://doi.org/10.1016/j.ijantimicag.2020.105924>
- [2] Chen, Y., Liu, Q., & Guo, D. (2020). Emerging coronaviruses: genome structure, replication, and pathogenesis. *Journal of medical virology*, 92(4), 418-423. <https://doi.org/10.1002/jmv.25681>
- [3] Singh, A. K., Singh, A., Shaikh, A., Singh, R., & Misra, A. (2020). Chloroquine and hydroxychloroquine in the treatment of COVID-19 with or without diabetes: A systematic search and a narrative review with a special reference to India and other developing countries. *Diabetes & Metabolic Syndrome: Clinical Research & Reviews*, 14(3), 241-246. <https://doi.org/10.1016/j.dsx.2020.03.011>
- [4] Ghosh, R., Chakraborty, A., Biswas, A., & Chowdhuri, S. (2021). Evaluation of green tea polyphenols as novel coronavirus (SARS CoV-2) main protease (Mpro) inhibitors—an in silico docking and molecular dynamics simulation study. *Journal of Biomolecular Structure and Dynamics*, 39(12), 4362-4374. <https://doi.org/10.1080/07391102.2020.1779818>
- [5] Boopathi, S., Poma, A. B., & Kolandaivel, P. (2021). Novel 2019 coronavirus structure, mechanism of action, antiviral drug promises and rule out against its treatment. *Journal of Biomolecular Structure and Dynamics*, 39(9), 3409-3418. <https://doi.org/10.1080/07391102.2020.1758788>
- [6] Grum-Tokars, V., Ratia, K., Begaye, A., Baker, S. C., & Mesecar, A. D. (2008). Evaluating the 3C-like protease activity of SARS-Coronavirus: recommendations for standardized assays for drug discovery. *Virus Research*, 133(1), 63-73. <https://doi.org/10.1016/j.virusres.2007.02.015>
- [7] Harcourt, B. H., Jukneliene, D., Kanjanahaluethai, A., Bechill, J., Severson, K. M., Smith, C. M., ... & Baker, S. C. (2004). Identification of severe acute respiratory syndrome coronavirus replicase products and characterization of papain-like protease activity. *Journal of virology*, 78(24), 13600-13612. <https://doi.org/10.1128/JVI.78.24.13600-13612.2004>
- [8] Osman, E. E. A., Toogood, P. L., & Neamati, N. (2020). COVID-19: living through another pandemic. *ACS Infectious Diseases*, 6(7), 1548-1552. <https://doi.org/10.1021/acsinfecdis.0c00224>
- [9] Yan, L., Velikanov, M., Flook, P., Zheng, W., Szalma, S., & Kahn, S. (2003). Assessment of putative protein targets derived from the SARS genome. *FEBS letters*, 554(3), 257-263. [https://doi.org/10.1016/S0014-5793\(03\)01115-3](https://doi.org/10.1016/S0014-5793(03)01115-3)
- [10] Yao, X., Ye, F., Zhang, M., Cui, C., Huang, B., Niu, P., Liu, X. & Liu, D. (2020). In vitro antiviral activity and projection of optimized dosing design of hydroxychloroquine for the treatment of severe acute respiratory syndrome coronavirus 2 (SARS-CoV-2). *Clinical infectious diseases*, 71(15), 732-739. <https://doi.org/10.1093/cid/ciaa237>
- [11] Grimstein, M., Yang, Y., Zhang, X., Grillo, J., Huang, S. M., Zineh, I., & Wang, Y. (2019). Physiologically based pharmacokinetic modeling in regulatory science: an update from the US Food and Drug Administration's Office of Clinical Pharmacology. *Journal of pharmaceutical sciences*, 108(1), 21-25. <https://doi.org/10.1016/j.xphs.2018.10.033>

- [12] Devaux, C. A., Rolain, J. M., Colson, P., & Raoult, D. (2020). New insights on the antiviral effects of chloroquine against coronavirus: what to expect for COVID-19?. *International journal of antimicrobial agents*, 55(5), 105938. <https://doi.org/10.1016/j.ijantimicag.2020.105938>
- [13] Warren, T. K., Jordan, R., Lo, M. K., Ray, A. S., Mackman, R. L., Soloveva, V., ... & Bavari, S. (2016). Therapeutic efficacy of the small molecule GS-5734 against Ebola virus in rhesus monkeys. *Nature*, 531(7594), 381-385. <https://doi.org/10.1038/nature17180>
- [14] Sheahan, T. P., Sims, A. C., Leist, S. R., Schäfer, A., Won, J., Brown, A. J., & Baric, R. S. (2020). Comparative therapeutic efficacy of remdesivir and combination lopinavir, ritonavir, and interferon beta against MERS-CoV. *Nature communications*, 11(1), 222. <https://doi.org/10.1038/s41467-019-13940-6>
- [15] Uddin, M. N., Ahmed, S. S., & Alam, S. R. (2020). Biomedical applications of Schiff base metal complexes. *Journal of Coordination Chemistry*, 73(23), 3109-3149. <https://doi.org/10.1080/00958972.2020.1854745>
- [16] Awual, M. R. (2015). A novel facial composite adsorbent for enhanced copper (II) detection and removal from wastewater. *Chemical Engineering Journal*, 266, 368-375. <https://doi.org/10.1016/j.cej.2014.12.094>
- [17] Awual, M. R. (2017). New type mesoporous conjugate material for selective optical copper (II) ions monitoring & removal from polluted waters. *Chemical Engineering Journal*, 307, 85-94. <https://doi.org/10.1016/j.cej.2016.07.110>
- [18] Awual, M. R. (2017). Novel nanocomposite materials for efficient and selective mercury ions capturing from wastewater. *Chemical Engineering Journal*, 307, 456-465. <https://doi.org/10.1016/j.cej.2016.08.108>
- [19] Awual, M. R., Rahman, I. M., Yaita, T., Khaleque, M. A., & Ferdows, M. (2014). pH dependent Cu (II) and Pd (II) ions detection and removal from aqueous media by an efficient mesoporous adsorbent. *Chemical Engineering Journal*, 236, 100-109. <https://doi.org/10.1016/j.cej.2013.09.083>
- [20] Awual, M. R., Hasan, M. M., Khaleque, M. A., & Sheikh, M. C. (2016). Treatment of copper (II) containing wastewater by a newly developed ligand based facial conjugate materials. *Chemical Engineering Journal*, 288, 368-376. <https://doi.org/10.1016/j.cej.2015.11.108>
- [21] Awual, M. R., & Hasan, M. M. (2019). A ligand based innovative composite material for selective lead (II) capturing from wastewater. *Journal of Molecular Liquids*, 294, 111679. <https://doi.org/10.1016/j.molliq.2019.111679>
- [22] INA, F., & SSBE, A. (2021). COVID vaccines and kids: five questions as trials begin. *Nature*, 592. [doi: https://doi.org/10.1038/d41586-021-01061-4](https://doi.org/10.1038/d41586-021-01061-4)
- [23] Kupferschmidt K. (2021) New coronavirus variants could cause more reinfections, require updated vaccines. [doi:10.1126/science.abg6028](https://doi.org/10.1126/science.abg6028)
- [24] Chen, L. R., Wang, Y. C., Lin, Y. W., Chou, S. Y., Chen, S. F., Liu, L. T., Wu, Y.T., Kuo, C.J & Juang, S. H. (2005). Synthesis and evaluation of isatin derivatives as effective SARS coronavirus 3CL protease inhibitors. *Bioorganic & Medicinal Chemistry Letters*, 15(12), 3058-3062. <https://doi.org/10.1016/j.bmcl.2005.04.027>
- [25] Mojzych, M., & Sebel, M. (2015). Synthesis and biological activity evaluation of schiff bases of 5-acyl-1, 2, 4-triazine. *Journal of the Chemical Society of Pakistan*, 37(2). [ISSN: 0253-5106](https://doi.org/10.1016/j.cej.2015.04.027)
- [26] Uddin, M. N., Amin, M. S., Rahman, M. S., Khandaker, S., Shumi, W., Rahman, M. A., & Rahman, S. M. (2021). Titanium (IV) complexes of some tetra-dentate symmetrical bis-Schiff bases of 1, 6-hexanediamine: Synthesis, characterization, and in silico prediction of potential inhibitor against coronavirus (SARS-CoV-2). *Applied Organometallic Chemistry*, 35(1), e6067. <https://doi.org/10.1002/aoc.6067>
- [27] Uddin, M. N., Chowdhury, D. A., & Rony, M. M. (2014). Complexes of Schiff bases derived from 2-hydroxyaldehyde and propane-1, 2-diamine: synthesis, characterization and antibacterial screening. *Am J chem appl*, 1, 12-18. [ISSN: 2381-4535](https://doi.org/10.1002/aoc.6067)

- [28] Chowdhury DA, Uddin MN, Chowdhury GK. (2006) Synthesis and characterization of some dioxomolybdenum(VI) complexes of Schiff bases with ONNO donor ligands. *The Chittagong Univ. J. Sci.*, 30(1):85 - 88. [ISSN 1561-1167](#)
- [29] Uddin, M. N., Salam, M. A., & Siddique, M. A. B. (2014). Complexes of VO₃⁺ with dibasic tetradentate Schiff bases and their microbial studies. *American Journal of Chemistry and Applications*, 1(2), 19-27. [ISSN Online: 2381-4535](#)
- [30] Gleeson, M. P., & Gleeson, D. (2009). QM/MM calculations in drug discovery: a useful method for studying binding phenomena?. *Journal of chemical information and modeling*, 49(3), 670-677. <https://doi.org/10.1021/ci800419j>
- [31] Hertwig, R. H., & Koch, W. (1997). On the parameterization of the local correlation functional. What is Becke-3-LYP?. *Chemical Physics Letters*, 268(5-6), 345-351. [https://doi.org/10.1016/S0009-2614\(97\)00207-8](https://doi.org/10.1016/S0009-2614(97)00207-8)
- [32] Frisch MJ, Trucks GW, Schlegel HB, Scuseria GE, Robb M, Cheeseman JR, et al. (2009) Gaussian 09, Revision D.01. Inc. Wallingford, CT.
- [33] Pearson, R. G. (1995). The HSAB principle—more quantitative aspects. *Inorganica Chimica Acta*, 240(1-2), 93-98. [https://doi.org/10.1016/0020-1693\(95\)04648-8](https://doi.org/10.1016/0020-1693(95)04648-8)
- [34] Pearson, R. G. (1986). Absolute electronegativity and hardness correlated with molecular orbital theory. *Proceedings of the National Academy of Sciences*, 83(22), 8440-8441. <https://doi.org/10.1073/pnas.83.22.8440>
- [35] Sussman, J. L., Lin, D., Jiang, J., Manning, N. O., Prilusky, J., Ritter, O., & Abola, E. E. (1998). Protein Data Bank (PDB): database of three-dimensional structural information of biological macromolecules. *Acta Crystallographica Section D: Biological Crystallography*, 54(6), 1078-1084. <https://doi.org/10.1107/S0907444998009378>
- [36] DeLano WL. (2002) The PyMOL Molecular Graphics System. Delano Scientific, San Carlos. <http://www.pymol.org>.
- [37] Guex, N., & Peitsch, M. C. (1997). SWISS-MODEL and the Swiss-Pdb Viewer: an environment for comparative protein modeling. *electrophoresis*, 18(15), 2714-2723. <https://doi.org/10.1002/elps.1150181505>
- [38] Uzzaman, M., & Uddin, M. N. (2019). Optimization of structures, biochemical properties of ketorolac and its degradation products based on computational studies. *DARU Journal of Pharmaceutical Sciences*, 27, 71-82. <https://doi.org/10.1007/s40199-019-00243-w>
- [39] Dallakyan, S., & Olson, A. J. (2015). Small-molecule library screening by docking with PyRx. *Chemical biology: methods and protocols*, 243-250. https://doi.org/10.1007/978-1-4939-2269-7_19
- [40] Version ADS 4.0. (2017) Accelrys, San Diego, USA.
- [41] Filimonov, D. A., Lagunin, A. A., Glorizova, T. A., Rudik, A. V., Druzhilovskii, D. S., Pogodin, P. V., & Poroikov, V. V. (2014). Prediction of the biological activity spectra of organic compounds using the PASS online web resource. *Chemistry of Heterocyclic Compounds*, 50, 444-457. <https://doi.org/10.1007/s10593-014-1496-1>
- [42] Khurana, N., Ishar, M. P. S., Gajbhiye, A., & Goel, R. K. (2011). PASS assisted prediction and pharmacological evaluation of novel nicotinic analogs for nootropic activity in mice. *European journal of pharmacology*, 662(1-3), 22-30. <https://doi.org/10.1016/j.ejphar.2011.04.048>
- [43] Cheng, F., Li, W., Zhou, Y., Shen, J., Wu, Z., Liu, G., Lee, P.W. & Tang, Y. (2012). admetSAR: a comprehensive source and free tool for assessment of chemical ADMET properties. <https://doi.org/10.1021/ci300367a>
- [44] Garbett, N. C., & Chaires, J. B. (2012). Thermodynamic studies for drug design and screening. *Expert opinion on drug discovery*, 7(4), 299-314. <https://doi.org/10.1517/17460441.2012.666235>

- [45] Lien, E. J., Guo, Z. R., Li, R. L., & Su, C. T. (1982). Use of dipole moment as a parameter in drug–receptor interaction and quantitative structure–activity relationship studies. *Journal of pharmaceutical sciences*, 71(6), 641-655. <https://doi.org/10.1002/jps.2600710611>
- [46] Sato, R., Vohra, S., Yamamoto, S., Suzuki, K., Pavel, K., Shulga, S., Blame, Y. & Kurita, N. (2020). Specific interactions between tau protein and curcumin derivatives: Molecular docking and ab initio molecular orbital simulations. *Journal of Molecular Graphics and Modelling*, 98, 107611. <https://doi.org/10.1016/j.jmgm.2020.107611>
- [47] Saravanan S, Balachandran V. (2014) Quantum chemical studies, natural bond orbital analysis and thermodynamic function of 2,5-dichlorophenylisocyanate. *Spectrochim. Acta Part A Mol. Biomol. Spectrosc.* 120:351-364. <https://doi.org/10.1016/j.saa.2013.10.042>
- [48] Hagar, M., Ahmed, H. A., Aljohani, G., & Alhaddad, O. A. (2020). Investigation of some antiviral N-heterocycles as COVID 19 drug: molecular docking and DFT calculations. *International Journal of Molecular Sciences*, 21(11), 3922. <https://doi.org/10.3390/ijms21113922>
- [49] Azam, F., Alabdullah, N. H., Ehmedat, H. M., Abulifa, A. R., Taban, I., & Upadhyayula, S. (2018). NSAIDs as potential treatment option for preventing amyloid β toxicity in Alzheimer’s disease: An investigation by docking, molecular dynamics, and DFT studies. *Journal of Biomolecular Structure and Dynamics*, 36(8), 2099-2117. <https://doi.org/10.1080/07391102.2017.1338164>
- [50] Murray JS, Politzer P. (2003) In *Comput. Med. Chem. for Drug Discovery*, CRC Press, pp. 231–254.
- [51] Nouredine, O., Issaoui, N., & Al-Dossary, O. (2021). DFT and molecular docking study of chloroquine derivatives as antiviral to coronavirus COVID-19. *Journal of King Saud University-Science*, 33(1), 101248. <https://doi.org/10.1016/j.jksus.2020.101248>
- [52] Yu, R., Chen, L., Lan, R., Shen, R., & Li, P. (2020). Computational screening of antagonists against the SARS-CoV-2 (COVID-19) coronavirus by molecular docking. *International Journal of Antimicrobial Agents*, 56(2), 106012. <https://doi.org/10.1016/j.ijantimicag.2020.106012>
- [53] Narkhede, R. R., Cheke, R. S., Ambhore, J. P., & Shinde, S. D. (2020). The molecular docking study of potential drug candidates showing anti-COVID-19 activity by exploring of therapeutic targets of SARS-CoV-2. *Eurasian Journal of Medicine and Oncology*, 4(3), 185-195. DOI: 10.14744/ejmo.2020.31503
- [54] Uddin, M. N., Siddique, Z. A., Akter, J., Rahman, M. S., Shumi, W., & Nasiruddin, M. (2022). Synthesis, molecular modeling, and biomedical applications of oxovanadium (IV) complexes of Schiff bases as a good SARS-CoV-2 inhibitor. *Inorganic and Nano-Metal Chemistry*, 52(6), 819-834. <https://doi.org/10.1080/24701556.2021.1952261>
- [55] Uzzaman, M., Junaid, M., & Uddin, M. N. (2020). Evaluation of anti-tuberculosis activity of some oxotitanium (IV) Schiff base complexes; molecular docking, dynamics simulation and ADMET studies. *SN Applied Sciences*, 2, 1-11. <https://doi.org/10.1007/s42452-020-2644-0>
- [56] Walum, E. (1998). Acute oral toxicity. *Environmental health perspectives*, 106(suppl 2), 497-503. <https://doi.org/10.1289/ehp.98106497>
- [57] Gleich, A., Kaiser, B., Honscha, W., Fuhrmann, H., & Schoeniger, A. (2019). Evaluation of the hepatocyte-derived cell line BFH12 as an in vitro model for bovine biotransformation. *Cytotechnology*, 71, 231-244. <https://doi.org/10.1007/s10616-018-0279-4>
- [58] Sanguinetti, M. C., & Tristani-Firouzi, M. (2006). hERG potassium channels and cardiac arrhythmia. *Nature*, 440(7083), 463-469. <https://doi.org/10.1038/nature04710>